RSC Advances

ROYAL SOCIETY OF CHEMISTRY

www.rsc.org/advances

Concentration-dependent effective attractions between PEGylated nanoparticles

Malin Zackrisson Oskolkova,*[a] Anna Stradner,[a] Jeanette Ulama,[b] and Johan Bergenholtz[a,b]

Received Xth XXXXXXXXXX 20XX, Accepted Xth XXXXXXXXX 20XX
First published on the web Xth XXXXXXXXXX 200X
DOI: 10.1039/b000000x

Effective attractions between colloidal particles bearing a grafted poly(ethylene glycol) (PEG) layer in water have been studied and quantified by measurements of the collective diffusion coefficient and by quantitative analysis of small-angle neutron scattering (SANS) data. Results for the collective diffusion coefficient in the dilute limit indicate that effective attractions develop gradually as carbonate anions are added to the dispersions. Analysis of SANS data within a square-well interaction model at a constant salt concentration allows for quantitative analysis of scattering patterns of samples prior to crossing into an aggregation regime, where particles form large clusters, reached either through increasing the temperature or the particle concentration. Aggregation is observed visually and is also evident in the scattering as a lowering of the intensity at intermediate wavevectors while leaving enhanced scattering in the forward direction, suggesting a nearby fluid-fluid phase transition. In addition, at low and moderate particle concentrations the attraction strength is shown to depend mainly on temperature but at high particle concentrations a much stronger temperature dependence is observed, which shows that the attraction acquires a dependence on particle concentration at sufficiently high concentrations. The concentration dependence is attributed to a decreased solvation of PEG chains due to an increased ratio of ethylene oxide segments to water.

1 Introduction

Addition of polymers, either free in solution, adsorbed, or grafted, to colloidal systems is an effective tool for regulating the interactions of colloidal particles. The resulting dispersion behavior and phases encountered in the phase diagram depend to a large extent on the properties of the added polymer. For non-adsorbing polymers, free in solution, an effective attraction, known as a depletion attraction, is induced; it is controlled by the polymer to particle size ratio and the concentration of polymer. The resulting phase diagram has been extensively studied[1] and one encounters a fluid-fluid phase separation, crystallization, and glass and gel formation[2–5]. It is mainly the range of the attraction which governs the phase or state diagram[1,6].

For polymers grafted on surfaces of nano- and microparticles the purpose is usually to produce a steric barrier against aggregation[7]. In this way particles can be made that are stable at extremely high salt concentrations[8] and that redisperse after centrifugation and freeze drying[9]. In addition, to enhance particle stability in biomedical and drug delivery applications it is common to use particles with grafted poly(ethylene glycol) (PEG), commonly referred to as PEGylated particles, and PEG derivatives, due to their long-time circulatory properties and biocompatibility[10–12]. Such steric layers on particles has even been found to affect the biodistribution of particles[13].

Even though PEG-covered particles, including PEGylated liposomes and emulsion drops, are generally considered as ideal systems from a biomedical point of view, their behavior is expected to depend on the physicochemical environment through the so-called solvent quality. For instance, for PEGylated particles, the solvent quality is governed by temperature and concentrations of certain salts that affect the solubility of PEG in aqueous solution. In this way, when the solvent quality for the PEG-graft is worsened, e.g., by raising the temperature, the particles begin to attract one another. Such interactions, should they become too strong, can lead to aggregation, which is generally quite detrimental in applications. However, from a model-system standpoint the state of the system can in this way be finely tuned to uncover how such interactions develop and act to destabilize the system. With related dispersions, comprising polymer-grafted silica particles in organic solvents, similar changes in solvent quality can lead to attractions and gel formation[14–16]. The attractions have in this case been linked to dramatic changes in the microstructure of the polymer corona, in which the polymer appears to crystallize[17–19].

The purpose of the present work is to examine the generality of these findings. To this end, we have studied dispersions of polymer-grafted particles that differ from the silica systems in

[a] *Division of Physical Chemistry, Center of Chemistry and Chemical Engineering, Lund University, SE-22100 Lund, Sweden. Fax: +46-46-222 4413; Tel: +46-46-222 8185; E-mail: malin.zackrisson@fkem1.lu.se*
[b] *Department of Chemistry and Molecular Biology, University of Gothenburg, Kemivägen 10, SE-41296 Göteborg, Sweden.*

a few key ways. The particles have been grafted with PEG and are dispersed in aqueous solution. Because both PEG and water interact via hydrogen bonds, the solvent quality is worsened by increasing the temperature. As a consequence, attractions are induced on increasing the temperature, which eventually leads to aggregation. However, to work at a range of temperatures that is not too far away from room temperature, we add sodium carbonate which also worsens the solvent quality for the PEG graft[20]. Although, in this study, we have to work at high concentrations of salt to observe significant effects, a lower degree of PEGylation would likely lead to similar effects setting in at lower salt concentrations. The particle core-shell morphology and hard-sphere-like interactions under good solvent conditions have been characterized extensively for these systems by small-angle neutron scattering (SANS)[21]. The dynamics and rheology have also been charted in quite some detail, when the particles are mutually repulsive, up to high concentrations where a glass transition governs much of the behavior[22].

In what follows, we focus on states close to where the particles begin to aggregate. The colloidal microstructure is examined by SANS, which, when combined with a structure factor model, also allows for characterization of the interaction. Measurements of the collective diffusion coefficient demonstrate that attractions are gradually introduced and strengthened upon adding salt. For sufficiently strong attractions, particles aggregate reversibly along a fairly sharp boundary. The scattering spectra in this region are consistent with precritical fluctuations signaling the presence of a nearby fluid-fluid phase transition. Furthermore, and the main finding of this work, the SANS analysis shows that the effective attraction not only depends on temperature but that it acquires a dependence on the particle concentration when the dispersions reach high concentrations. Such high concentrations are routinely encountered in coatings and film-forming applications[23,24].

2 Experimental

2.1 Materials

The colloidal system investigated here consists of poly(ethylene glycol)-grafted polystyrene particles dispersed in water. As a background electrolyte, 6.15 mM NaCl+3.85 mM NaN_3 was employed throughout to make sure that any surface charges are screened and to prevent bacterial growth during longer-time storage. Further details of the synthesis, cleaning, and characterization have been given previously[21] and will only be summarized briefly here. The particles were synthesized in a one-step co-polymerization between styrene and methoxy poly(ethylene glycol) acrylate (mPEG-2000-acrylate) using potassium persulfate as initiator, following the procedure devised by Brindley *et al.*[25]. This protocol produces sterically stabilized, non-deuterated spherical latex particles with a well-defined core-shell structure interacting via hard-sphere-like interactions at room temperature in 10 mM salt solution[21,22]. Concentrated dispersions were obtained by centrifugal filtration (Pall, Gelman Lab.) to desired high mass content. The final weight fractions of stock dispersions were determined by drying in an oven at 60°C and subsequently converted to particle mass concentrations c (g/mL) using measured particle densities (DMA5000 density meter, Anton Paar). Conversion to an effective hard-sphere volume fraction $\phi_{\rm HS}$ made use of the following relation, $\phi_{\rm HS} = 1.632c - 0.086c^2 - 1.281c^3$, previously determined by SANS analysis[22]. Additional salt, Na_2CO_3, was added in the form of concentrated solution to latices to obtain final compositions with respect to salt and particles.

2.2 3D-Dynamic light scattering

Dynamic light scattering (DLS) measurements were performed using the 3D cross-correlation technique[26,27] on a 3D single-mode fiber goniometer system (LS Instruments, Fribourg, Switzerland) equipped with a Flex correlator and a diode laser with a wavelength of 680.4 nm. The temperature was set by a circulating water bath to 25.0°C and a scattering angle θ of 90° was maintained in all measurements shown here. However, angular scans, covering $30° < \theta < 130°$, were performed to confirm the q-independence of the apparent diffusion coefficient such that the measurements were performed in the collective diffusion regime[28]. Here, $q = (4\pi n/\lambda)\sin\theta/2$ is the magnitude of the wave vector, given in terms of the solvent refractive index n and the laser-light wavelength *in vacuo* λ. To suppress multiple scattering further, high-quality NMR tubes with a diameter of 5 mm (Armar AG, Switzerland) were used as sample cells in order to shorten the light path.

2.3 Small-angle neutron scattering

SANS experiments were carried out at the SANSI facility at the Swiss neutron source SINQ at the Paul Scherrer Institut (PSI) in Villigen, Switzerland. For the SANS measurements a neutron wavelength $\lambda = 8$ Å and a wavelength spread ($\Delta\lambda/\lambda$) of 10% were used. A sample-to-detector distance of 20 meters and a collimation length of 18 m were used, yielding an accessible q range of 0.025–0.37 $\rm nm^{-1}$. All measurements were carried out under particle core contrast, using a solvent composition of 80/20 w/w H_2O/D_2O, resulting in a negligible scattering contribution from the PEG graft. Samples were prepared in stoppered quartz cells of 1 mm path length (Hellma, Germany). The temperature was controlled by a circulating water bath and was monitored inside a representative sample in the thermostated sample holder. The raw scattering spec-

tra were corrected for background from the solvent, sample cell, electronic noise, and transmission by conventional procedures. Furthermore, the two-dimensional isotropic scattering spectra were azimuthally averaged and converted to absolute intensities by using water as a standard.

3 Results and discussion

The purpose of this work is to investigate the nature of the effective attractions that are induced under marginal and poor solvent conditions for the PEG-graft of sterically stabilized polystyrene particles. We have previously shown that addition of a few hundred mM of Na_2CO_3 to aqueous dispersions of similar PEG-grafted particles produces small structural changes in the PEG layer which translate in moderate attractions among colloids[21]. Whereas adding larger quantities of Na_2CO_3 to dilute dispersions results in aggregation, addition of other salts, like NaCl, is ineffectual in this respect and particles remain stable, at least at room temperature[8,21]. Qualitatively, this behavior follows the clouding properties of free PEG polymer in aqueous electrolyte solutions[20].

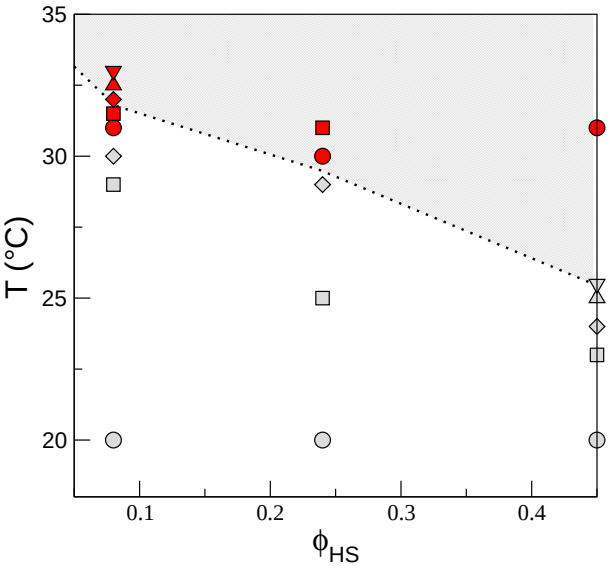

Fig. 1 The behavior of dispersions of PEG-grafted polystyrene spheres in 400 mM aqueous solutions of Na_2CO_3 as a function of particle concentration and temperature as assessed by visual observation. The particles aggregate at elevated temperatures (shaded region). The symbols denote states for which SANS measurements have been collected. The symbols correspond to those in Fig. 3 and serve as a key to the temperatures used in the SANS measurements. The grey symbols show states for which the recorded SANS intensities could be modeled with equilibrium theory and filled (red) symbols show states for which a similar modeling was not possible (cf. Sec. 3.2).

Figure 1 expands somewhat on the stability aspect of these dispersions, by showing the result of varying the temperature and particle concentration at a constant Na_2CO_3 concentration of 400 mM. On increasing the temperature, particles aggregate at a rather sharply defined point where the samples become grainy, indicating the formation of large flocs, which was also confirmed in the more dilute samples by light microscopy. The aggregates redisperse when the sample is cooled. This behavior is consistent with early observations made by Vincent and co-workers of the reversible aggregation of larger PEG-grafted polystyrene particles[29,30]. They refer to the transition as a critical flocculation temperature or concentration, depending on how the transition is approached. They rationalized this behavior, especially the fact that the boundary depends on temperature and concentration, as caused by a fluid-fluid transition due to a weak effective attraction between particles. Similar observations hold for non-aqueous dispersions of sterically stabilized particles[15,31–35], except that aggregation occurs on lowering the temperature. In addition, at least for the non-aqueous dispersions in the dilute part of the phase diagram, it seems that the transition is connected to incipient phase separation because the dense phase in these systems, if it can be observed at all, corresponds to a dynamically arrested structure and not to an equilibrium fluid phase[14]. In what follows, we probe the interactions that lead to such transitions in these aqueous systems, beginning with dilute particle concentrations and continuing with more concentrated systems.

3.1 Attractions investigated by dynamic light scattering

Dynamic light scattering (DLS) measurements have been made on fairly dilute samples as a function of particle and Na_2CO_3 concentration. However, when the solvent quality for the PEG graft worsens, it is necessary to take steps to avoid multiple scattering. For this reason 3D cross-correlation DLS (3D-DLS) has been employed[26,27]. Since the particles are small relative to the wavelength of light ($qa \approx 0.33$, where a is the radius of the particle core), DLS measurements probe large-scale spatial concentration fluctuations connected to the collective diffusion coefficient[28]. As has been recognized by van den Broeck and co-workers[36], the collective diffusion coefficient in the dilute limit can be used to distinguish to some extent between repulsive and attractive colloidal interactions, which has been exploited in studies of interactions in colloidal systems[37,38]. For systems in which pair-interactions are predominantly repulsive the collective diffusion coefficient increases with particle concentration. Attractions weaken the concentration dependence, and, for sufficiently strong attractions, the collective diffusion coefficient decreases with increasing particle concentration. In other words, repulsions among particles act to smooth out small concentration gradients more rapidly than in systems with additional attractions.

When the interaction potential is known, the dilute-limiting behavior of the collective diffusion coefficient can be calculated from theory [36,39,40].

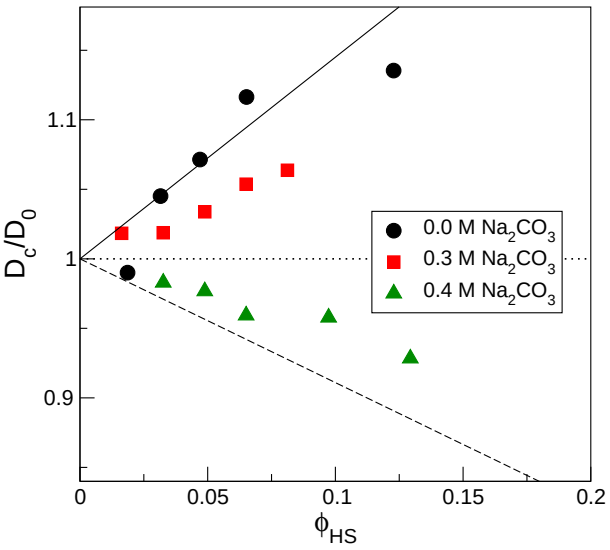

Fig. 2 Collective diffusion coefficient normalized by the single-particle diffusion coefficient as a function of effective hard-sphere volume fraction for increasing concentrations of added Na_2CO_3, as labeled. A constant temperature of 25°C was maintained throughout the measurements. Included are the results for hard spheres (solid line, $\lambda_c = 1.454$) and square-well particles with $B_2/B_2^{\rm HS}$=0.67 (dotted line, $\lambda_c = 0$). Also shown is a prediction for D_c for square-well particles using $B_2/B_2^{\rm HS}$=0.47 (dashed line, $\lambda_c = -0.93$), determined from a previous SANS analysis [21].

In Fig. 2 the collective diffusion coefficients, extracted from a second-order cumulant analysis of 3D-DLS intensity cross correlation function data, are shown as a function of particle concentration and Na_2CO_3 concentration. In the absence of extra added salt, i.e. under good solvent conditions, the collective diffusion coefficient increases with concentration, as expected for excluded-volume interactions and in good agreement with the leading-order hard-sphere result [39,40]: $D_c/D_0 = 1 + 1.454\phi_{\rm HS}$. Adding Na_2CO_3 produces divalent CO_3^{2-} ions in solution (pH ≈ 11.5), which decreases the solvent quality for the PEG graft. As a consequence, the collective diffusion coefficient exhibits a different concentration dependence, $D_c/D_0 = 1 + \lambda_c\phi_{\rm HS}$; it increases less strongly with concentration at lower levels of Na_2CO_3, but for a sufficiently high concentration of Na_2CO_3, as in Fig. 2 for 0.4 M Na_2CO_3, the dilute-limiting slope λ_c becomes negative. It is notable in Fig. 2 that the concentration dependence changes smoothly with the amount of added Na_2CO_3, such that the particle interactions can be tuned in a gradual manner from repulsive to attraction-dominated. In addition, we note that the attractions are present well below the boundary in Fig. 1 which marks visible aggregation.

For square-well interactions the dilute-limiting slope λ_c can be calculated for arbitrary well widths and well depths. Such calculations are summarized by $\lambda_c = -3.046 + 4.5B_2/B_2^{\rm HS}$, where $B_2/B_2^{\rm HS} = 1 - (\exp(\epsilon/k_BT) - 1)(R^3 - 1)$ is a reduced second virial coefficient in terms of the well depth ϵ, the thermal energy k_BT , and the dimensionless range of the interaction potential R. This result for the dilute-limiting slope λ_c holds numerically within a few percent for well widths even up to 40% of the radius for negative values of $B_2/B_2^{\rm HS}$, i.e. for moderate to strong attractions. This formula derives from the adhesive-sphere model [41] and it illustrates the fact that one cannot separate effects of well width and well depth based on the measurements in Fig. 2. In previous work [21] the attractions were characterized for similar particles using quantitative modeling of SANS data, which employed a square-well form for the attractive part of the interaction. For samples with [Na_2CO_3]=0.4 M and a temperature of 25°C this analysis yielded a reduced second virial coefficient, $B_2/B_2^{\rm HS} = 0.47$, which was independent of particle concentration up to $\phi_{\rm HS} \approx 0.31$ [21]. This magnitude of attraction can be seen to yield a negative slope in Fig. 2 in reasonable agreement with the measurements for these dispersions at this salt concentration. It should be noted that this prediction applies in the dilute limit, $\phi_{\rm HS} \to 0$, and the determination of λ_c experimentally necessitates defining an effective hard-sphere volume fraction, which is often a difficult matter [42]. Here, this was accomplished using a correlation obtained from a quantitative SANS analysis of the same system of particles under good solvent conditions over a large range of concentrations. There is one condition, however, that is free from any ambiguities deriving from the conversion of mass concentration to an effective hard-sphere volume fraction, the Boyle-like condition of zero slope. A collective diffusion coefficient with a zero initial slope requires $B_2/B_2^{\rm HS} = 0.67$. It follows that for [Na_2CO_3]=0.4 M, attractions of greater magnitude than those corresponding to this value are expected for all temperatures in excess of 25°C.

3.2 Attractions investigated by SANS

As demonstrated by the DLS results, adding increasing amounts of divalent carbonate anions smoothly introduces effective attractions of moderate strength at room temperature. The attractions were further strengthened by increasing the temperature. This was done while monitoring the microstructure with SANS both on approaching and crossing the aggregation boundary. In most cases, rather than 'quenching' samples well into the aggregation regime, temperature was used to bring samples close to aggregation rather slowly, maintaining equilibrium as long as possible. In Fig. 3 the scattering inten-

sity is shown as a function of q and temperature for a sequence of volume fractions $\phi_{\rm HS} = 0.08$, 0.24, and 0.45, all in the presence of 0.4 M Na_2CO_3. The proximity of these samples to the aggregation boundary can be read off the diagram in Fig. 1, where state points corresponding to the SANS measurements are indicated.

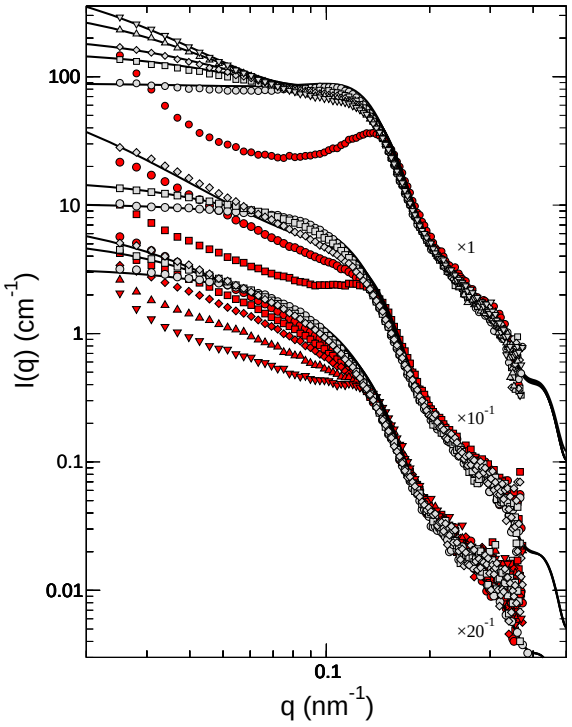

Fig. 3 Scattering intensity as a function of q and temperature for a set of three volume fractions, $\phi_{\rm HS} = 0.08$ (bottom group of data), $\phi_{\rm HS} = 0.24$ (middle), and $\phi_{\rm HS} = 0.45$ (top). All were dispersed in 0.4 M Na_2CO_3 and adjusted to core scattering conditions at 20/80 w/w D_2O/H_2O. The data have been shifted vertically for clarity (with shift factors given along the right-hand side). Data with grey symbols correspond to samples with no visible signs of aggregation below the aggregation boundary in Fig. 1, which, in addition, could be fitted with an equilibrium theory for a square-well model [21] as shown by the solid lines. Data with red symbols could not be fitted well or not at all with the same model. The symbols correspond to those in Fig. 1, allowing identification of the different temperatures of the measurements.

Some general trends are readily apparent from Fig. 3. As the aggregation regime is approached from the fluid phase by raising the temperature, the low-q scattering increases, as expected when attractions among particles increase in strength. This effect has previously been modeled for similar particle dispersions using a square-well attraction (for details see Ref. 21). We make use of the same model, which employs the Percus-Yevick (PY) theory for the structure factor necessary for modeling the scattering intensity of non-dilute samples. Core scattering conditions, corresponding to 20/80 w/w D_2O/H_2O, were employed to minimize the scattering from the PEG layer by approximately matching the scattering length density of it. The scattering is modeled using an average core radius of 21 nm, an average hard-sphere radius of 24 nm, a shell area coverage of 0.7, and a 16.5% polydispersity for all samples (see Ref. 21 for details). In this way the scattering intensity can be modeled quite well for temperatures approaching the aggregation regime. The low-q rise in intensity signals increased concentration fluctuations, suggesting that the samples come close to a fluid-fluid phase transition on raising the temperature, which appears to be located quite close to where aggregation sets in as detected visually. However, in the vicinity of the aggregation boundary the scattering intensity begins to behave differently compared to at the lower temperatures. As seen in Fig. 3, at intermediate q the intensity begins to decrease with increasing temperature (red symbols in Fig. 3), which, at sufficiently high temperatures, leaves a peak in the intensity at rather high q. These features are incompatible with the predictions of the structure factor model, which is based on equilibrium theory. Also, it seems that the scattering intensity at the lowest q remains quite high, which is certainly the case for the highest particle concentration deep in the aggregation regime. We note that sedimentation of particles out of the volume illuminated by the neutron beam would be associated with a systematic lowering of the intensity for all q [43]. This was observed at much lower concentrations, but it was not observed for $\phi_{\rm HS} \geq 0.08$, nor were any signs of delayed settling or collapse detected, as observed in other systems [43–45]. In addition, no intermediate-range structures, such as distinct particle clusters [46], are observed in these systems on the length scales probed by these SANS measurements. However, e.g., ultra-small-angle neutron scattering measurements would be required to provide a more definitive answer as to whether clusters appear prior to crossing into the aggregation regime.

Shah and co-workers [47] have made similar observations regarding scattering in connection with depletion-induced gelation. They were able to predict scattering intensities and structure factors using equilibrium theory on strengthening depletion attractions between particles to the point where systems gelled, but beyond gelation the scattering deviated from that predicted by equilibrium theory. They did observe enhanced low-q scattering similar to that seen here, but they did not note any decrease in the scattering intensity at intermediate q as observed here. Somewhat surprisingly, similar studies of non-aqueous dispersions of sterically stabilized particles, which one might have thought should be more akin to the PEG-grafted particle systems under study here, did not find any low-q upturn in the scattering at higher concentrations where the attractions were strong enough to gel the samples [16,48].

By fitting the SANS data with the square-well model, the

magnitude of the attraction can be extracted as a function of temperature and particle concentration. However, as with the DLS measurements, the analysis does not yield separate estimates of the well width and well depth. For this reason the results have been converted to an overall measure of the strength of attraction as given by the reduced second virial coefficient, $B_2/B_2^{\rm HS}$. Results for the reduced second virial coefficient of the square-well potential obtained from the SANS analysis are summarized in Table 1 and shown in Fig. 4. Essentially all the other parameters in the analysis were kept constant in all fits of the SANS spectra. The exception was at the highest volume fraction of $\phi_{\rm HS}$=0.45 for which the effective hard-sphere diameter was set to 0.98, whereas in all other cases it was kept at unity. This had a small effect on the quality of the fits, but it was nonetheless included due to the fact that PEG-brushes are likely to become compressed at such high concentrations. The results for the second virial coefficient, which show that $B_2/B_2^{\rm HS}$ becomes increasingly negative with increasing temperature irrespective of the particle concentration, demonstrate that attractions persist among particles at [Na_2CO_3]=0.4 M and that these attractions increase in strength as the temperature is increased. Compared to the strength of attraction obtained from the analysis of the DLS data at 400 mM Na_2CO_3 at 25°C, for which $B_2/B_2^{\rm HS} = 0.56$ is consistent with the negative slope of the data in Fig. 2, the SANS analysis yields a stronger attraction.

Table 1 The reduced second virial coefficient of the square-well interaction used to model the SANS data in Fig. 3 for the three particle concentrations investigated. Temperatures at which samples had passed into the aggregation regime are referred to as 'agg'. All samples were dispersed in 0.4 M Na_2CO_3, in core scattering, i.e. 20/80 w/w D_2O/H_2O. A reduced second virial coefficient of $B_2/B_2^{\rm HS} = 1$ corresponds to hard-sphere behavior.

T (°C)	$B_2/B_2^{\rm HS}$		
	$\phi_{\rm HS} = 0.08$	$\phi_{\rm HS} = 0.24$	$\phi_{\rm HS} = 0.45$
20.0	0.2	0.5	0.4
23.0	-	-	-0.2
24.0	-	-	-0.5
25.0	-	0.1	-1.0
25.5	-	-	-1.5
29.0	-0.7	-1.0	agg.
30.0	-1.1	agg.	agg.

The main result from this analysis is that for the two less concentrated systems, $\phi_{\rm HS} = 0.08$ and 0.24, $B_2/B_2^{\rm HS}$ shows a similar dependence on temperature, whereas for the more concentrated one, $\phi_{\rm HS} = 0.45$, $B_2/B_2^{\rm HS}$ shows a far stronger temperature dependence. In other words, as the temperature is increased, the attractions grow more rapidly when the system is concentrated. As remarked before, in a previous SANS study carried out for similar particles at constant temperature [21], it was noted that the scattering intensity could be modeled with a $B_2/B_2^{\rm HS}$ value that was independent of particle concentration up to $\phi_{\rm HS} \approx 0.31$. This study concerns far stronger attractions at higher temperatures and includes a more concentrated dispersion at $\phi_{\rm HS} = 0.45$. The behavior reported in Fig. 1, which shows that the system, when concentrated, aggregates at much lower temperatures is consistent with the results for $B_2/B_2^{\rm HS}$. In fact, given the rise in the low-q intensity in Fig. 3 and the strong temperature dependence of $B_2/B_2^{\rm HS}$ in Fig. 4, a fluid-fluid spinodal transition should be located at around 27°C for $\phi_{\rm HS} = 0.45$. Examining the behavior of sterically stabilized silica in organic solvent at similarly high particle concentrations, reinforces the differences in behavior compared to this PEGylated system. Whereas the aggregation observed here is connected with negative values of $B_2/B_2^{\rm HS}$, the gelation observed at high concentrations in the non-aqueous system occurs at positive values [48].

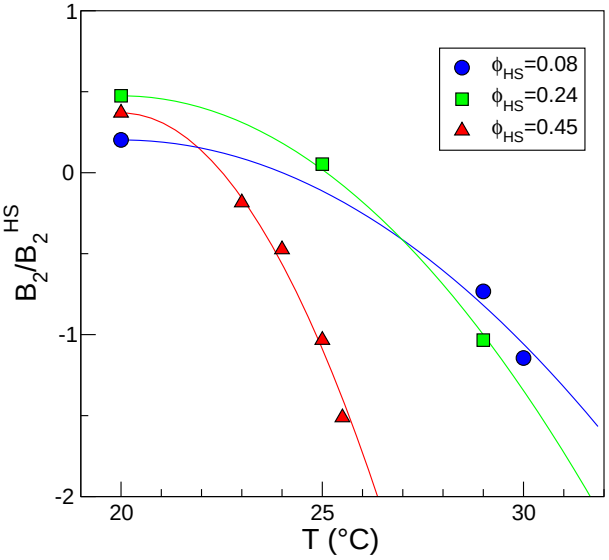

Fig. 4 The reduced second virial coefficient of the square-well interaction extracted from the SANS analysis as a function of temperature for the three different particle concentrations corresponding to $\phi_{\rm HS}$=0.08, 0.24 and 0.45, as labeled. Solid lines serve only as guides to eye.

To rationalize this behavior we note that moderate attractions between polymer-grafted particles with high grafting density are to be expected when the solvent quality is worsened [49]. Moreover, the magnitude of this attraction, judging from computer simulations [49], appears to be a smooth function of solvent quality and is associated with a gradual shortening and densification of the grafted brush, which translates into a

shift of the attraction to shorter separations. The former is in qualitative agreement with the findings of this study, whereas a shift of the attraction by a few nanometers at most is too small to be ascertained from the SANS analysis. The finding of the much stronger temperature dependence of the attraction at high particle concentrations indicates that the interactions become concentration dependent at sufficiently high particle concentrations. A possible explanation for this behavior is that the grafted PEG chains compete for hydrogen bonding to water molecules. As the particle concentration reaches high values, so does effectively the PEG concentration at the expense of the concentration of the solvent. In modeling the phase behavior of bulk PEG solutions, Matsuyama and Tanaka[50] developed a model in which solvent molecules associate with chains such that the concentration of free, non-associated solvent depends on both temperature and polymer concentration. In this way closed-loop phase diagrams of aqueous PEG solutions could be predicted that in addition shows that the polymer solvation decreases both as the temperature and the polymer concentration increase. We speculate that this is the origin of the stronger attractions seen here at higher particle concentrations.

4 Conclusions

The effective attraction and static structure of aqueous dispersions of PEGylated nanoparticles have been studied as a function of solvent quality and particle concentration. Adding divalent ions combined with increasing the temperature serve to reduce the solvency of the PEG graft and produces effective attractions among colloids. When the attractions become sufficiently strong macroscopic aggregation ensues reversibly along a relatively sharp boundary. This process is signaled by a systematic enhancement of the low-q scattering followed by a decrease of intermediate-range structural correlations, pointing to an inhomogeneous structure beyond the point of aggregation as observed also visually. The SANS analysis reveals that the attraction is independent of particle concentration for low to moderate particle concentrations, where it is only governed by the temperature. However, for high particle concentrations a much stronger temperature dependence is found, which also shows that the attraction becomes dependent on the particle concentration. This behavior of the attraction is attributed to a decreased polymer solvation at higher particle concentrations where also PEG concentrations are high, albeit confined to the particle surfaces, such that the ratio of ethylene oxide segments to water becomes high.

5 Acknowledgments

We thank the Swiss spallation source at the Paul Scherrer Institut (PSI), Villigen, Switzerland, for beam time and we thank our local contact S. van Petegem for help and assistance with using the SANS facility.

References

1 S. M. Ilett, A. Orrock, W. C. K. Poon and P. N. Pusey, *Phys. Rev. E*, 1995, **51**, 1344–1352.
2 E. H. A. de Hoog, W. K. Kegel, A. van Blaaderen and H. N. W. Lekkerkerker, *Phys. Rev. E*, 2001, **64**, 021407.
3 K. Pham, A. M. Puertas, J. Bergenholtz, S. U. Egelhaaf, A. Moussaid, P. N. Pusey, A. B. Schofield, M. E. Cates, M. Fuchs and W. C. K. Poon, *Science*, 2002, **296**, 104–106.
4 K. N. Pham, S. U. Egelhaaf, P. N. Pusey and W. C. K. Poon, *Phys. Rev. E*, 2004, **69**, 011503.
5 S. Manley, H. M. Wyss, K. Miyazaki, J. C. Conrad, V. Trappe, L. J. Kaufman, D. R. Reichman and D. A. Weitz, *Phys. Rev. Lett.*, 2005, **95**, 238302.
6 A. P. Gast, C. K. Hall and W. B. Russel, *J. Colloid Interface Sci.*, 1983, **96**, 251–267.
7 D. H. Napper, *Polymeric stabilization of colloidal dispersions*, Academic Press, London, 1983.
8 J. Ulama, M. Z. Oskolkova and J. Bergenholtz, *J. Phys. Chem. B*, 2014, **118**, 2582–2588.
9 D. Burger, J. Gisin and E. Bartsch, *Colloids Surf. A*, 2014, **442**, 123–131.
10 A. L. Klibanov, K. Maruyama, V. P. Torchilin and L. Huang, *FEBS Lett.*, 1990, **268**, 235–237.
11 S. E. Dunn, A. Brindley, S. S. Davis, M. C. Davies and L. Illum, *Pharm. Res.*, 1994, **11**, 1016–1022.
12 T. M. Allen and P. R. Cullis, *Science*, 2004, **303**, 1818–1822.
13 S. S. Davis, L. Illum, S. M. Moghimi, M. C. Davies, C. J. H. Porter, I. S. Muir, A. Brindley, N. M. Christy, M. E. Norman, P. Williams and S. E. Dunn, *J. Controlled Release*, 1993, **24**, 157–163.
14 H. Verduin and J. K. G. Dhont, *J. Colloid Interf. Sci.*, 1995, **172**, 425–437.
15 C. J. Rueb and C. F. Zukoski, *J. Rheology*, 1997, **41**, 197–218.
16 S. Ramakrishnan, V. Gopalakrishnan and C. F. Zukoski, *Langmuir*, 2005, **21**, 9917–9925.
17 C. G. de Kruif and J. C. van Miltenburg, *J. Chem. Phys.*, 1990, **93**, 6865–6869.
18 S. Roke, J. Buitenhuis, J. C. van Miltenburg, M. Bonn and A. van Blaaderen, *J. Phys.: Condens. Matter*, 2005, **17**, S3469–S3479.
19 S. Roke, O. Berg, J. Buitenhuis, A. van Blaaderen and M. Bonn, *Proc. Natl. Acad. Sci. (USA)*, 2006, **103**, 13310–13314.
20 K. P. Ananthapadmanabhan and E. D. Goddard, *Langmuir*, 1987, **3**, 25–31.
21 M. Zackrisson, A. Stradner, P. Schurtenberger and J. Bergenholtz, *Langmuir*, 2005, **21**, 10835–10845.
22 M. Zackrisson, A. Stradner, P. Schurtenberger and J. Bergenholtz, *Phys. Rev. E*, 2006, **73**, 011408.
23 J. L. Keddie, *Mat. Sci. Eng.*, 1997, **21**, 101–170.
24 D. R. Bassett, *J. Coatings Tech.*, 2001, **73**, 43–55.
25 A. Brindley, S. S. Davis, M. C. Davies and J. F. Watts, *J. Colloid Interf. Sci.*, 1995, **171**, 150–161.
26 E. Overbeck, C. Sinn, T. Palberg and K. Schätzel, *Colloids Surf. A*, 1997, **122**, 83–87.
27 C. Urban and O. Schurtenberger, *J. Colloid Interf. Sci.*, 1998, **207**, 150–158.
28 W. B. Russel and A. B. Glendinning, *J. Chem. Phys.*, 1981, **74**, 948–952.

29 C. Cowell, R. Li-In-On and B. Vincent, *J. Chem. Soc., Faraday Trans.*, 1978, **74**, 337–347.

30 C. Cowell and B. Vincent, *J. Colloid Interf. Sci.*, 1982, **87**, 518–526.

31 J. W. Jansen and A. Vrij, *J. Colloid Interf. Sci.*, 1986, **114**, 481–491.

32 M. Chen and W. B. Russel, *J. Colloid Interf. Sci.*, 1991, **141**, 564–577.

33 M. C. Grant and W. B. Russel, *Phys. Rev. E*, 1993, **47**, 2606–2614.

34 C. J. Rueb and C. F. Zukoski, *J. Rheology*, 1998, **42**, 1451–1476.

35 A. P. R. Eberle, N. J. Wagner and R. Castaneda-Priego, *Phys. Rev. Lett.*, 2011, **106**, 105704.

36 C. van den Broeck, F. Lostak and H. N. W. Lekkerkerker, *J. Chem. Phys.*, 1981, **74**, 2006–2010.

37 M. Zackrisson, R. Andersson and J. Bergenholtz, *Langmuir*, 2004, **20**, 3080–3089.

38 A. Y. Mirarefi and C. F. Zukoski, *J. Cryst. Growth*, 2004, **265**, 274–283.

39 G. K. Batchelor, *J. Fluid Mech.*, 1976, **74**, 1–29.

40 B. Cichocki and B. U. Felderhof, *J. Chem. Phys.*, 1988, **89**, 1049–1054.

41 B. Cichocki and B. U. Felderhof, *J. Chem. Phys.*, 1990, **93**, 4427–4432.

42 W. C. K. Poon, E. R. Weeks and C. P. Royall, *Soft Matter*, 2012, **8**, 21–30.

43 D. Pontoni, S. Finet, T. Narayanan and A. R. Rennie, *J. Chem. Phys.*, 2003, **119**, 6157–6165.

44 J. R. Weeks, J. S. van Duijneveldt and B. Vincent, *J. Phys.: Condens. Matter*, 2000, **12**, 9599–9606.

45 L. Starrs, W. C. K. Poon, D. J. Hibberd and M. M. Robins, *J. Phys.: Condens. Matter*, 2002, **14**, 2485–2505.

46 A. Stradner, H. Sedgwick, F. Cardineaux, W. C. K. Poon, S. U. Egelhaaf and P. Schurtenberger, *Nature*, 2004, **432**, 492–495.

47 S. A. Shah, Y.-L. Chen, S. Ramakrishnan, K. S. Schweizer and C. F. Zukoski, *J. Phys.: Condens. Matter*, 2003, **15**, 4751–4778.

48 A. P. R. Eberle, R. Castaneda-Priego, J. M. Kim and N. J. Wagner, *Langmuir*, 2012, **28**, 1866–1878.

49 F. LoVerso, S. E. Egorov and K. Binder, *Macromolecules*, 2012, **45**, 8892–8902.

50 A. Matsuyama and F. Tanaka, *Phys. Rev. Lett.*, 1990, **65**, 341–344.